THE JOURNAL OF BIOLOGICAL CHEMISTRY VOL. 285, NO. 49, pp. 38141–38148, December 3, 2010

Vesicle Fusion Probability Is Determined by the Specific Interactions of Munc18*[S]

Received for publication, July 16, 2010, and I revised form, August 17, 2010 Published, JBC Papers in Press, August 26, 2010, DOI 10.1074/jbc.M110.164038

Annya M. Smyth[‡], Colin Rickman[§], and Rory R. Duncan[‡1]

From the [‡]Centre for Integrative Physiology, University of Edinburgh, George Square, Edinburgh EH8 9XD and the [§]School of Engineering and Physical Sciences, Department of Chemistry, Heriot Watt University, Edinburgh EH14 4AS, United Kingdom

Mammalian-regulated secretion is absolutely dependent on four evolutionarily conserved proteins: three SNARE proteins and munc18. Dissecting the functional outcomes of the spatially organized protein interactions between these factors has been difficult because of the close interrelationship between different binding modes. Here, we investigated the spatial distribution of single munc18 molecules at the plasma membrane of cells and the underlying interactions between syntaxin and munc18. Disruption of munc18 binding to the N-terminal peptide motif of syntaxin did not alter munc18 localization on the plasma membrane but had a pronounced influence on the behavior of secretory vesicles and their likelihood to undergo fusion. We therefore conclude that interaction with the syntaxin N-peptide can confer differential release probabilities to secretory vesicles and may contribute to the delineation of secretory vesicle pools.

In all specialized secretory cells, regulated exocytosis is mediated by three central players; the vesicular membrane protein synaptobrevin (v-SNARE) and plasma membrane proteins SNAP-25 (synaptosome-associated protein 25 kDa) and syntaxin (t-SNAREs) (1, 2). Helices from each of these proteins interact to form a stable, ternary four-helical SNARE complex which catalyzes the fusion of vesicular and plasma membranes (3). The regulation of SNARE assembly is dependent upon the presence of a range of highly conserved accessory proteins, which are known to modulate SNARE function (4–6). One such family are the evolutionarily conserved Sec1p/Munc18 (SM)[2] proteins (7). Evidence from multiple studies has indicated that this family of accessory proteins plays a central role in SNARE trafficking (8–11), docking of secretory vesicles (12, 13), and in modulating the final membrane fusion steps (14, 15).

Munc18-1, a mammalian SM counterpart (7), was originally defined as an inhibitor of neurotransmitter release as it was observed to sequester syntaxin from forming the SNARE fusion complex (16, 17). This hypothesis was at odds with genetic experiments, which suggested a more positive role for munc18 (for review, see Ref. 18). It has now been established that munc18 is absolutely required for membrane fusion, most probably through its direct partnership with syntaxin (19–21). Munc18 is able to interact with syntaxin in three possible conformations. First, Munc18 can bind and stabilize syntaxin in a "closed" conformation in which the Habc domain of syntaxin folds back and occludes the SNARE motif (mode 1) (16, 17). Second, interaction via the syntaxin highly conserved N terminus (mode 2) was recently confirmed, in common with other SM proteins (4, 22–27). Third, munc18 can also interact with the ternary SNARE complex via "open" syntaxin (mode 3) (24–26). Modes 2 and 3 utilize the same N-terminal binding motif in syntaxin and differ in the conformation and additional interactions adopted by the syntaxin molecule. More recently, it was suggested that munc18 interacts with the v-SNARE synaptobrevin *in vitro*, albeit at a far lower affinity than that observed for syntaxin (28).

The multiple munc18-syntaxin binding mechanisms are utilized in distinct cellular locations and perform different regulatory roles (26). Mode 1 binding is important in facilitating the trafficking of syntaxin to the plasma membrane (9) whereas modes 2 and 3 are involved in vesicle mobilization (21), SNARE complex binding (24), regulating the rate of membrane fusion in *vitro* (25), and in synaptic vesicle "priming" (29). Importantly, despite a large effort focused on the roles of munc18 in the exocytotic pathway it still remains unknown how munc18 is organized on the plasma membrane at the molecular level and how it may act upon single vesicles prior to the final fusion event.

We describe new rationally designed mutants of munc18 that quantifiably disrupt specifically mode2/3 interaction *in vitro* and in living cells and use this as a tool to define the spatially restricted functional effects of this interaction. Using superresolution microscopy we have defined the highest possible resolution mapping of munc18 molecular distribution at the neuroendocrine plasma membrane. Together, these experiments demonstrate that munc18 molecules, interacting with the N terminus of syntaxin1, greatly increase the fusion competence of a specific pool of mode2 interaction-proximal vesicles.

EXPERIMENTAL PROCEDURES

Vectors and Cell Culture—Plasmids encoding glutathione *S*-transferase (GST) fusion proteins with syntaxin1a (amino acids 1–261, cytoplasmic domain), syntaxin (amino acids 7–261, N-terminal truncation) were described previously (26), and syntaxin (amino acids 1–225, ionic layer truncation) was constructed using similar techniques. A plasmid encoding a polyhistidine-tagged munc18 (amino acids 1–594) and

* This work was funded by Wellcome Trust and Medical Research Council project grant awards (to R. R. D. and C. R.).

⌘ *Author's Choice*—Final version full access.

[S] The on-line version of this article (available at http://www.jbc.org) contains supplemental Figs. 1–4.

[1] To whom correspondence should be addressed. Tel.: 44 131 6502864; Fax: 44 131 6503128; E-mail: rory.duncan@ed.ac.uk.

[2] The abbreviations used are: SM, Sec1p/Munc18; FLIM, fluorescence lifetime imaging microscopy; NPY, neuropeptide Y; PALM, photoactivatable localization microscopy; TCSPC, time-correlated single-photon counting; TIRFM, total internal reflection fluorescence microscopy; EYFP, enhanced Yellow Fluorescent protein.

munc18([E132A], [E132K], [I127A], [I127F], [D112A], or [D112K]) was as described previously (30). Generation of syntaxin1a N-terminal truncations was performed by PCR and subsequent ligation into HindIII/KpnI and HindIII/XbaI sites of pmCerulean-C1 and PGEXKG, respectively. The [E132A], [E132K], [I127A], [I127F], [D112A], and [D112K] mutations were generated individually by site-directed mutagenesis of munc18 in pGEX-KG and pEYFP-N1 vectors using a QuikChange II XL kit (Stratagene). Munc18 siRNA PC-12 cells (KD43) were a kind gift of Shuzo Sugita (10) and grown in RPMI 1640 medium supplemented with 10% horse serum, 5% fetal bovine serum, 10 mM Glutamax (Invitrogen), 50 μg/ml gentamicin, puromycin (2. 5 μg/ml) and maintained at 37 °C in 7.5% (v/v) CO_2, 92.5% (v/v) air. Transfections were performed using Lipofectamine 2000 (Invitrogen).

Protein Biochemistry—Recombinant GST fusion proteins were expressed and purified as described previously (31). For *in vitro* binding reactions, 2 μg of GST-syntaxin1 and truncated syntaxin (1–225), (1–188), and (7–261) were immobilized on glutathione-Sepharose beads (GE Healthcare) and incubated in a total volume of 100 μl of 20 mM Tris-HCl, pH 7.4, 100 mM NaCl, 1 mM EDTA, 0.1% Triton X-100 (buffer A). Beads were washed by low speed centrifugation, and bound protein eluted in SDS-containing sample buffer followed by SDS-PAGE and Coomassie staining. For binding reactions involving munc18, purified GST-syntaxin1a and truncations were incubated with either freshly prepared detergent rat brain extract, as described previously (26), or with freshly prepared detergent bacterial extract containing expressed recombinant His6-munc18 or a mutant form. The homogenate was then applied to GST-syntaxin beads and washed three times in buffer A, and bound protein was analyzed by Western immunoblotting using a monoclonal anti-munc18 antibody (BD Biosciences) and West Dura enhanced chemiluminescence kit (Pierce). The protein sequence alignment was generated using the ConSurf Data base (32), and the structure was rendered using PyMOL (33).

Confocal Laser Scanning Microscopy and Live Cell Maintenance—Cells with the lowest detectable expression levels were selected for analysis, and levels were similar between experiments. All time-correlated single-photon counting (TCSPC) experiments were performed using a Zeiss LSM 510 Axiovert confocal laser scanning microscope, equipped with a pulsed excitation source (MIRA 900 Ti:Sapphire femtosecond pulsed laser with a coupled VERDI 10-watt pump laser (Coherent). Data were acquired using a 1024 × 1024-pixel image size, using a Zeiss Plan NeoFLUAR 1.4 NA ×63 oil immersion lens or a Zeiss C-Apochromat 1.2 NA ×63 water-corrected immersion objective lens For all microscopy, live cells imaged were maintained at 37 °C in 5% (v/v) CO_2, 95% (v/v) air in a POC chamber (LaCon).

TCSPC-Fluorescence Lifetime Imaging Microscopy (FLIM) Acquisition and Analysis—TCSPC measurements were made under 800–820-nm two-photon excitation, which efficiently excited cerulean, without any detectable direct excitation or emission from EYFP, using a fast photomultiplier tube (H7422; Hamamatsu Photonics UK) coupled directly to the rear port of the Axiovert microscope. Full-frame TCSPC recordings were acquired for between 30 s and 60s, with mean photon counts between 105 and 106 counts/second. Images were recorded at 256 × 256 pixels from a 1024 × 1024-pixel image scan with 256 time bins over a 12-ns period. Off-line FLIM data analysis used pixel-based fitting software (SPCImage, Becker and Hickl). The optimization of the fit parameters was performed by using the Levenberg-Marquardt algorithm, minimizing the weighted χ^2 quantity. As controls for nonspecific FRET, or FRET between GFPs that may form dimers spontaneously when overexpressed in cells, we determined the fluorescence lifetime of cerulean-Syx1–288 alone. No FRET was detected in any of these control experiments.

Vesicle Tracking and Fusion—For vesicle tracking and fusion experiments cells were imaged under total internal reflection fluorescence microscopy (TIRFM) illumination using an Olympus CellR widefield TIRFM microscope equipped with a 488-nm and 561-nm diode laser. Data were acquired using a Hamamatsu ImageEM EMCCD using an Olympus PLAN APO 1.45 NA ×150 oil immersion objective. TIRFM data of munc18-silenced PC-12 cells (KD43) expressing NPYmGFP (21), or neuropeptide Y (NPY) mCherry (21), as required, maintained at 37 °C in 5% (v/v) CO_2, 95% (v/v) air, were acquired with a pixel size of 106 nm at 20 Hz. Single vesicles were identified and tracked using Imaris 5 (Bitplane). All track lengths shorter than 10 frames were discarded from the quantification. Where required, cells were stimulated by the addition of ATP to a final concentration of 300 μM. To quantify the amount of exocytosis, the number of fusing vesicles was calculated as a percentage of the total number of labeled vesicles at the plasma membrane.

Photoactivatable Localization Microscopy (PALM)—All munc18-silenced PC-12 cells (KD43) were transfected with munc18 (or variant) fused to PACherry and fixed with 4% (w/v) paraformaldehyde. Cycles of brief activation at 405 nm, followed by rapid imaging in TIRF mode at 561 nm were performed using an Olympus IX-81 microscope equipped with Olympus CellR acquisition software and an ImageEM EM-CCD 512 × 512 camera (Hamamatsu UK). All PALM imaging used an Olympus UAPO 1.45 NA ×150 oil lens with a resulting pixel size of 106 nm. Activation and bleaching steps in each cycle were optimized to ensure a sparse distribution of single molecules were activated and bleached during each cycle. PALM data analysis was performed using Matlab routines written by Dr. Samuel Hess (Maine).

RESULTS

Dissection of Munc18-Syntaxin Interaction Mode in Vitro and in Cells—To determine the mode of munc18-syntaxin binding employed in our experiments we needed to design targeted mutations to disrupt each type of interaction specifically. The approach we used was to examine the amino acid sequence of members of the SM protein family. Evolutionary conservation of amino acids, with relation to the three-dimensional protein structure is indicative of an essential function (34). We aligned the amino acid sequence of 191 predicted SM proteins, mapping the degree of conservation on to the crystal structure of munc18 bound to syntaxin1 (27) (Fig. 1*A*). This approach highlighted the amino acids lining the mode 2/3 binding pocket on munc18 and indicated Glu^{132} and Asp^{112} (expected to form

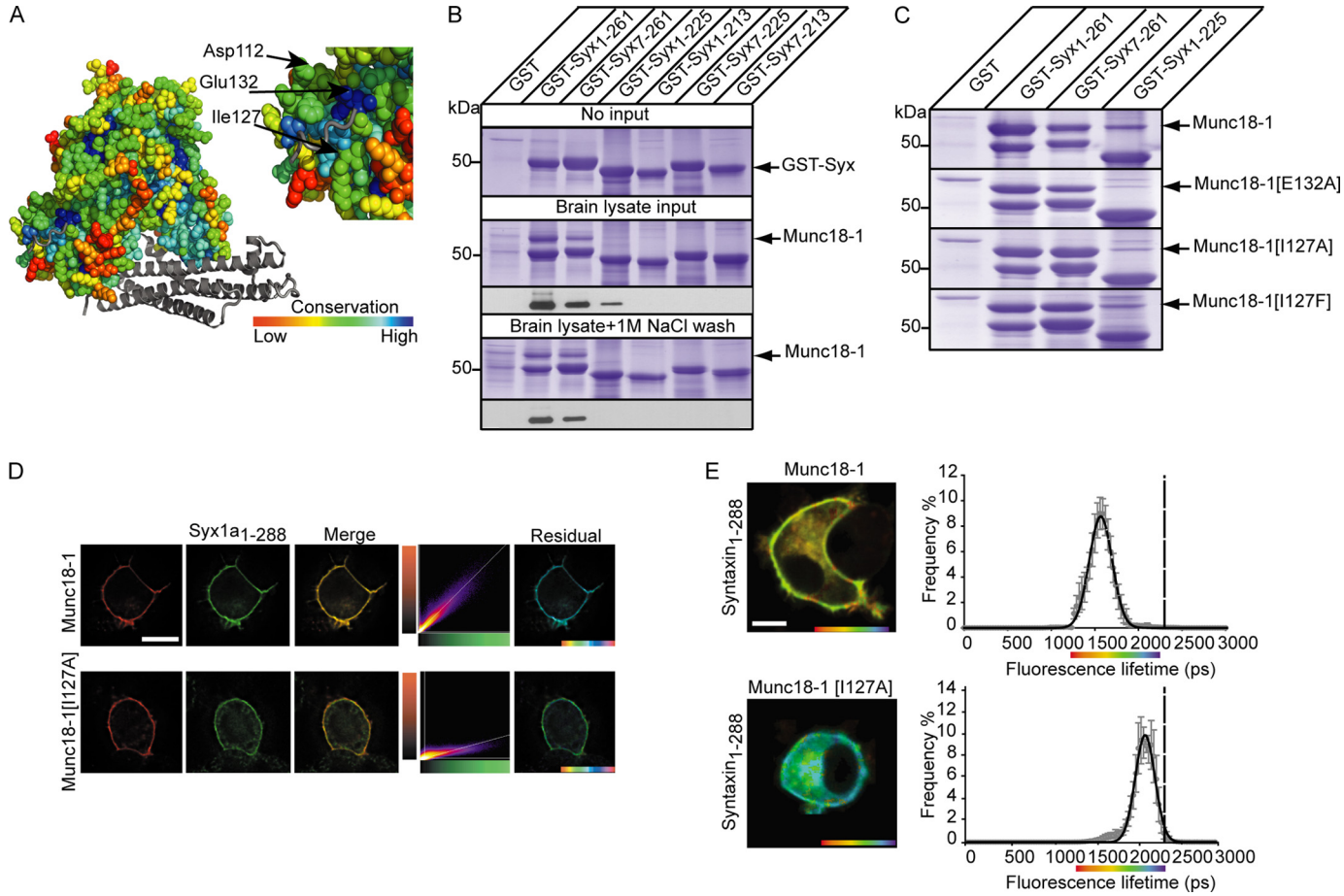

FIGURE 1. **Targeted disruption of mode 2/3 interaction both *in vitro* and in live cells.** *A*, structural alignment of munc18 (based on crystal structure PDB 3C98) (27) bound to syntaxin (gray helices) with amino acid conservation are shown on a *color-coded scale* (*red*, low; *blue*, high conservation; *left panel*). Amino acids Asp[112], Glu[132], and Ile[127], predicted to disrupt N-terminal binding, are *highlighted* on an *enlarged view* (*right panel*). *B*, truncation of the N terminus [Syx7–261] (to inhibit mode 2/3 binding and/or removal of the ionic layer [Syx1–225] of syntaxin (to inhibit mode 1 binding) did not eliminate binding to native munc18. The combination of these truncations or removal of the entire SNARE helix of syntaxin [Syx1–213] eliminated detectable binding to munc18. Mode 2/3 binding to syntaxin [Syx1–255] was sensitive to a high ionic strength wash. Bound material was analyzed by SDS-PAGE and Coomassie staining or Western blotting. *C*, GST-Syx7–261 and GST-Syx1–225 were immobilized on glutathione-Sepharose beads and incubated with bacterial lysate containing His_6-munc18 or its mutant forms. Bound material was analyzed by SDS-PAGE and Coomassie staining. *D*, EYFP-munc18–1[I127A] resulted in a significant change in the fluorescence co-variance with mCer-syntaxin. Wild type or EYFP-munc18-1[I127A] (*red*) and mCer-Syx (*green*) were expressed in munc18-1 silenced PC-12 cells (KD43) and imaged by confocal laser scanning microscopy and subsequent image data deconvolution. The *merge image* shows areas of coincidence in *yellow hues*. The two-dimensional *histogram* represents the intensity for each channel in each voxel with a *color scale* representing frequency. The residual map displays weighted residuals from the line fit to the histogram, thus indicating fluorescence channel co-variance. The *hue* is from −1 to 1 with *cyan* corresponding to a 0 residual. *Scale bar*, 5 μm. *E*, cerulean-Syx1–288, in the presence of EYFP-munc18, in munc18-1-silenced PC-12 cells (KD43), exhibited a plasma membrane and intracellular membrane distribution. The *color scale* represents the fluorescence lifetime, and brightness represents intensity. The weighted mean fluorescence lifetime values were plotted as a frequency distribution histogram (*right panels*) with a mean fluorescence lifetime of 1568 ± 131 ps (mean ± S.E., $n = 6$). Munc18[I127A] resulted in a quenching of the fluorescence lifetime to a lesser extent compared with wild type munc18 (*lower panels*). These data are plotted (*lower right panel*) and reveal a single lifetime of 2047 ± 133 ps (mean ± S.E., $n = 5$). The *dashed line* on both graphs represents the mean fluorescence lifetime of cerulean-Syx1–288 in the presence of unfused munc18 and EYFP (2321 ± 40 ps (mean ± S.E., $n = 10$; supplemental Fig. 1*B*). *Scale bar*, 5 μm, fluorescence lifetime *color bar* 1250 ps (*red*)–2250 ps (*blue*).

hydrogen bonds to the N-terminal motif of syntaxin1) and Ile[127] (forming one side of the hydrophobic pocket (27)) as being potentially important for this interaction. We constructed two-point mutations for each amino acid (I127A/I127F, E132A/E132K, and D112A/D112K) to investigate their individual contributions in binding syntaxin and the downstream functional role this binding mode could play.

To investigate the impact of these changes on syntaxin1-munc18 interactions *in vitro* it was necessary to be able to isolate mode 1 and mode 2/3 interactions biochemically. We have reported previously that truncation of the N terminus of syntaxin (GST-Syx7 261) can disrupt mode 2/3 interactions (26). To perturb mode 1 interactions we designed truncations of the SNARE helix of syntaxin based on the close interaction of this region with munc18 in mode 1 interactions (27). Two truncations were used: removal of the syntaxin C terminus up to the ionic layer of the SNARE helix (GST-Syx1–225) and a complete removal of the SNARE helix (GST-Syx1–213). To examine the influence of these mutations and their combinations, we incubated purified proteins with fresh brain lysate. Upon incubation, native munc18 readily bound to wild type syntaxin (GST-Syx1 261; Fig. 1*B*). Truncation of the N terminus of syntaxin (GST-Syx7–261) caused a small decrease in the amount of bound munc18 detected as a result of loss of mode 2/3 binding. Munc18 binding following truncation of syntaxin to the ionic layer (GST-Syx1–225) was also detected but at decreased levels

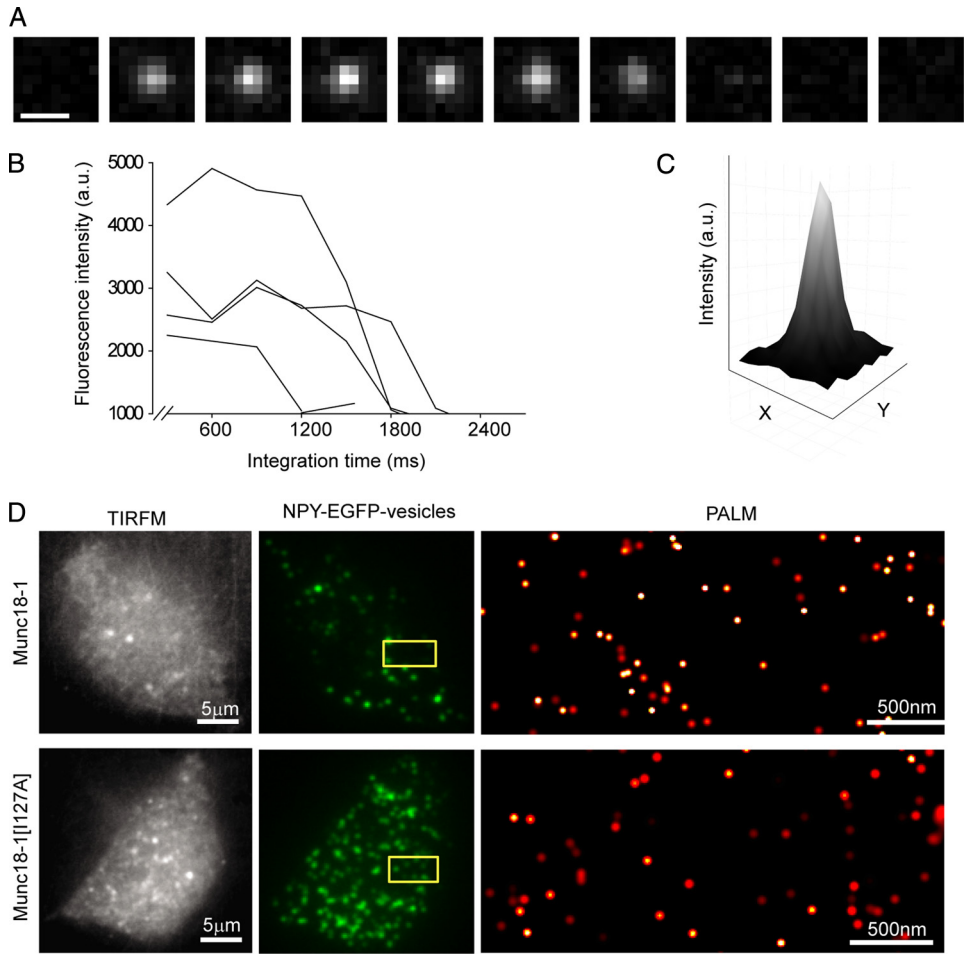

FIGURE 2. **Munc18 spatial distribution at the plasma membrane is unaffected by the mode of interaction.** *A*, sequential frames of a single molecule of PA-mCherry-labeled munc18 on the plasma membrane demonstrating the quantal activation and bleaching characteristic of single fluorescent molecules. Each frame is a 300-ms integration with fluorophore activation by brief 405-nm illumination preceding the *first frame*. *Scale bar*, 1 μm. *B*, intensity plot over time for representative molecule bleaching events. The 405-nm activation pulse immediately preceded the first time point. The relative intensity of each molecule and the period of time each molecule spends emitting photons are stochastic. Bleaching events are quantal. *C*, frames containing detectable fluorescence averaged and displayed as an intensity profile plot for the region. The peak in fluorescence equates to the size of the point spread function of the microscope. *D*, Munc18 (*upper*) and munc18[I127A] (*lower*) TIRFM image (*left*), TIRFM image showing NPY-EGFP-labeled secretory vesicles (*center*), and a rendered map of single munc18 molecules, in munc18-1-silenced PC-12 cells (KD43), within the *boxed region* at the plasma membrane (*right*).

as a result of loss of mode 1 binding. No interactions were detected following removal of the whole SNARE helix of syntaxin (GST-Syx1–213). Importantly, the combination of the N-terminal truncation and the ionic layer truncation (GST-Syx7–225) resulted in the complete removal of detectable munc18 binding through ablation of both binding modes. Mode 2/3 binding to GST-Syx1–225 was also eliminated in a high salt buffer, highlighting the considerable ionic nature of this interaction in contrast to the mode1 interaction (GST-Syx7–261).

To determine whether our munc18 point mutations disrupted specifically mode 2/3 interaction with syntaxin1, we incubated bacterial lysates containing His-tagged munc18, and mutant forms, with GST-syntaxin immobilized on beads (Fig. 1*C* and supplemental Fig. 1). GST-Syx7–261 was used to examine the impact of munc18 mutations on mode 1 binding and GST-Syx1–225 to assess perturbations of mode 2/3 binding. Mutations I127A, I127F, and E132A caused a reduction in the level of mode 2/3 binding compared with wild type syntaxin *in vitro*. To determine whether these mutants acted in a similar manner in a cellular context, we transfected munc18-silenced cells (KD43) (10) with siRNA-resistant fluorescent fusion proteins of munc18 and the above mutations in combination syntaxin1a. Fluorescence intensity covariance analysis in these cells confirmed that the three mutants that disrupted mode 2/3 interaction *in vitro* also had a significant effect on syntaxin intracellular localization, with munc18[I127A] having the largest influence (Fig. 1*D* and supplemental Fig. 2). For clarity in this paper, we therefore focus on this specific mutant to address downstream functional contributions; data describing all the other mutants we tested in all assays are in supplemental figures.

Mutations in the Hydrophobic Pocket of Munc18 Result in a Change in Its Interaction with Syntaxin at the Plasma Membrane—To determine where mode 2/3 interaction is predominately utilized within a cellular environment, we employed FLIM. FLIM quantifies the fluorescence lifetime of a fluorophore and can be a quantitative measure of Förster resonance energy transfer (FRET) between proximal (within 5 nm) acceptor and donor molecules (35). As a control, mCer syntaxin was expressed with unfused munc18 and EYFP, in KD43 PC-12 cells (supplemental Fig. 1; munc18-1-silenced cells were used for every cell-based experiment). This analysis revealed a principally plasma membrane localization of syntaxin with some labeling of intracellular compartments, as reported previously (9, 26). FLIM analysis showed a statistically significant quenching of the mean fluorescence lifetime of donor mCer-Syx1–266 from 2310 ± 151 ps (mean ± S.E., $n = 10$), in the absence of a proximal FRET acceptor, to 1563 ± 65 ps (mean ± S.E., $n = 6$) in the presence of EYFP-munc18 (Fig. 1*e*), indicative of FRET. This confirmed that munc18 and syntaxin interact on the plasma membrane. Munc18[I127A] resulted in significantly less quenching of the donor fluorescence lifetime to 2062 ± 70 ps (mean ± S.E., *t* test, $p < 0.05$, $n = 5$; Fig. 1*e* and supplemental Fig. 1), indicating either reduced interaction or altered conformation of interaction. Plotting every pixel in the image but assigning donor fluorescence lifetime value a color revealed

that areas on the plasma membrane contained significantly less energy transfer, confirming that mode 2/3 interaction predominates at the cell surface (Fig. 1*E*).

Molecular Distribution of Munc18 Molecules at the Plasma Membrane Is Unaffected by Mode of Interaction with Syntaxin—Having disrupted mode 2/3 interactions at the plasma membrane, we set out to determine whether this specific effect resulted in, or was caused by, a spatial reorganization of munc18 molecules. Munc18 has been localized on a gross microscopic scale to the plasma membrane of secretory cells several times (9, 26, 36), with this membrane association mediated principally by interaction with syntaxin (26). However, diffraction-limited imaging has a maximum lateral resolution of 178 nm (measured in our system) (9), too low to determine anything other than massive reorganization if this interaction is disrupted.

To localize single munc18 molecules across the plasma membrane we employed superresolution total internal reflection fluorescence PALM. This involved the serial activation, localization, and photodestruction of photoactivatable molecules at the plasma membrane (Fig. 2). Both wild type munc18 and munc18[I127A] exhibited a similar spatial distribution. Thus, targeted munc18 mutation to disrupt mode 2/3 interactions resulted only in a reorganization of interaction with syntaxin with no change in the spatial molecular pattern at the plasma membrane.

Mode of Interaction of Munc18 with Syntaxin Influences Vesicle Dynamics at the Plasma Membrane—We previously observed that phosphorylation of serine 14 in syntaxin disrupted mode 2/3 interaction with munc18, resulting in the increased average immobilization of secretory vesicles, rendering them unable to support membrane fusion (21). This agrees well with the notion that vesicular mobility is enhanced directly preceding fusion (37). Therefore, we investigated whether mutation of the munc18 hydrophobic pocket resulted in similar downstream effects, specifically on single vesicle kinetics and their fusion capabilities. To achieve this we again employed TIRFM to attain both high spatial and temporal resolution at the single-vesicle level (38). Employing our mutant proteins, alongside fluorescently labeled vesicles (NPY mCherry), we were able to measure multiple parameters at physiological temperatures.

These analyses revealed that disrupting mode 2/3 interaction (munc18[127A]) significantly restricted average vesicle displacement, speed, and track length compared with wild type munc18 in rescued silenced cells (Fig. 3, *A–C* and supplemental Fig. 3). To examine whether this change in vesicle behavior affected downstream membrane fusion, we next analyzed single-vesicle fusion events, using our pH-sensitive EGFP-NPY probe (Fig. 4*A*) (21). In the single-vesicle fusion assay, secretion is observed as a rapid transient increase in fluorescence intensity due to a change in the pH of the microenvironment upon fusion. In the absence of munc18, stimulated exocytosis was not significantly different from basal secretion in both population growth hormone release assays (data not shown) and in single-vesicle fusion TIRFM experiments, indicating a requirement for munc18 in exocytosis as observed previously (19). Exocytosis in silenced PC-12 cells was fully rescued (to levels observed in native PC12 cells) by introducing a fluorescent fusion of wild

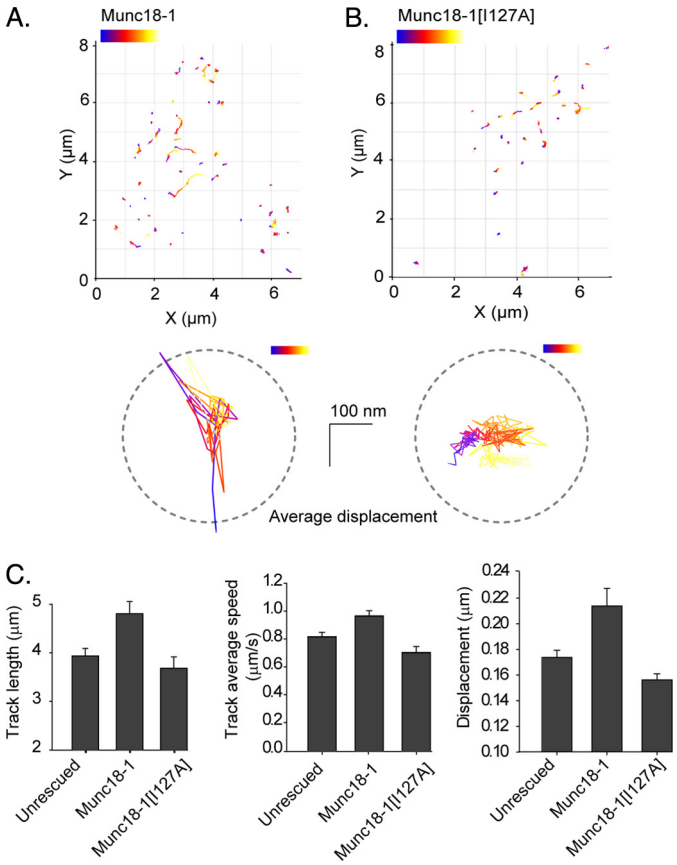

FIGURE 3. **Vesicle dynamics at the plasma membrane are modulated by munc18-syntaxin-N-terminal interaction.** *A* and *B*, fluorescent vesicles were tracked under TIRF illumination in munc18-silenced PC-12 cells (KD43) expressing wild type munc18 (*A*) or munc18[I127A] (*B*). Individual vesicle trajectories are shown as *tracks* with *color* corresponding to time during acquisition (*blue* (start) *to red* (end)). Examples most closely matching the mean track length for each condition are shown underneath each trajectory map. The *dashed circles* correspond to a vesicle diameter of 400 nm. *C*, individual tracks were measured for track length, mean vesicle speed, and vesicle track displacement (>250 tracks/cell, $n = 5$ cells). Rescue with munc18[I127A] resulted in reduced average track length, displacement and speed, indicative of a tighter tethering, compared with wild type munc18. *Error bars* are S.E. ($p < 0.05$, one-way ANOVA, $n = 5$).

type munc18 (Fig. 4*B*; in agreement with Ref. 10). Importantly, this indicates not only that our probes are functional, but that the number of munc18 molecules we found associated with plasma membrane (or not, as the case may be) is sufficient for full fusion capacity. However, exocytosis was only partially rescued by munc18[I127A] (Fig. 4*B*) (32% ± 1.8 (mean proportion of fused vesicles ± S.E., $n = 4$, significantly less than wild type: 51% ± 0.9, $n = 5$; $p < 0.05$, Mann-Whitney U).

To understand further the molecular interactions underlying this spatially restricted mode 2/3 interaction-enhanced exocytosis, we quantified the munc18-syntaxin interaction specifically at the base of the cell using FLIM. These data revealed that munc18-syntaxin interactions have membrane-proximal vesicles associated with all areas of the cell surface. Similar analysis employing munc18[I127A] reported the loss of detectable interaction in large areas of the cell surface (shown in *gray scale* in Fig. 4*C*); however, these areas were not avoided by membrane-proximal secretory vesicles. This finding indicates that mode 2/3 interaction is not required *per se* for vesicle-membrane association, at least within sub-100-nm axial distances.

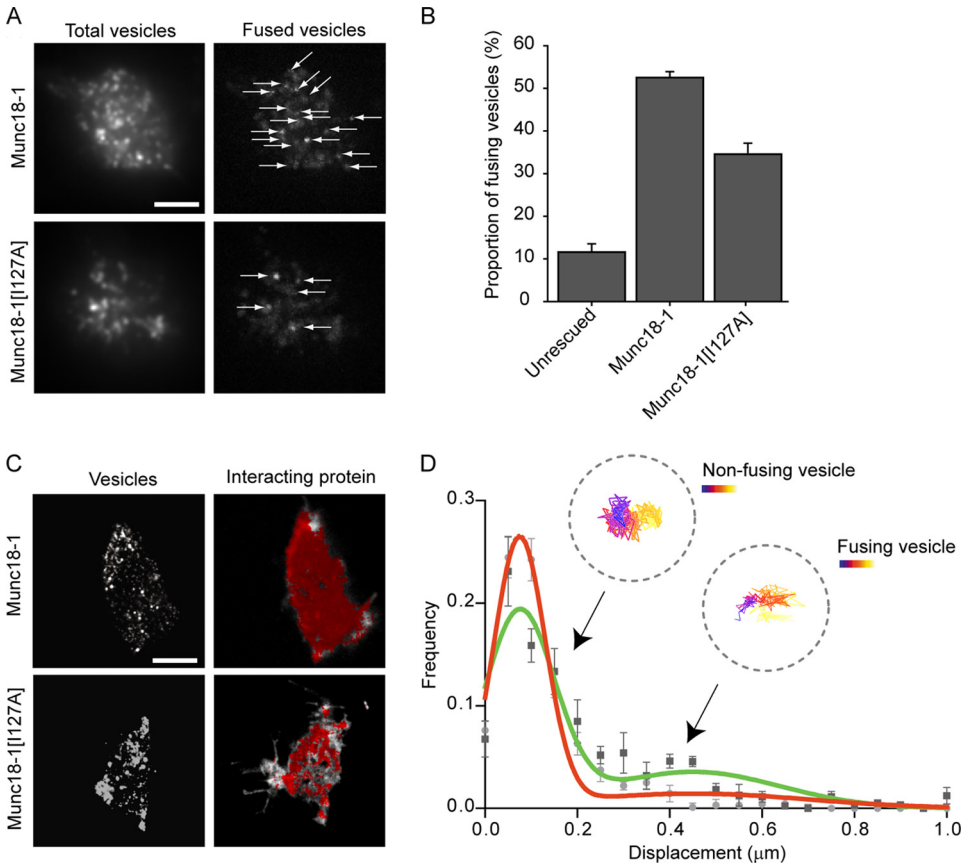

FIGURE 4. **N-terminal interactions increase the fusion likelihood in a specific pool of vesicles.** *A*, total number of labeled vesicles at the beginning of the experiment (*left panel*) compared with the number of fusion events (*right panel*) is shown. Individual fusion events were detected by analyzing the rate of fluorescence intensity change during the recording. *Arrows* indicate single-vesicle fusion events within munc18-1-silenced PC-12 cells (KD43) detected throughout the entire recording period of 3 min. Rescue with munc18[I127A] elicits fewer fusion events compared with wild type munc18. *B*, exocytosis is reduced by knockdown of munc18 and is partly rescued by munc18[I127A], compared with wild type munc18. Fusion events were calculated as the percentage of the total number of vesicles visible at the start of the recording that underwent fusion after stimulation with 300 μM ATP. *Error bars* are S.E. (one-way ANOVA, $n = 4$). *C*, FLIM was used to quantify interaction changes specifically at the plasma membrane upon disruption of N-terminal binding, correlated with vesicle position. FLIM maps reveal that munc18[I127A] decreases the amount of interaction detected, specifically within large areas at the plasma membrane (*right panels*). Pixels containing donor fluorescence lifetime values >2 SD below the mean, noninteracting control values obtained (supplemental Fig. 1*B*) are shown (*red*). Pixels containing donor fluorescence lifetime values consistent with noninteracting syntaxin are shown (*gray scale*). *D*, majority of nonfusing vesicles have a limited displacement distance whereas a second, more highly mobile pool of vesicles has an increased likelihood of exocytosis. Graph shows the measured vesicle displacements from wild type (*dark gray*) and munc18[I127A]-rescued cells (*light gray*), best fit by a double Gaussian function (wild type, *green*; [I127A], *red*). Both distributions are bimodal, with a significant decrease in the magnitude of the higher mobility, fusion-competent pool of vesicles in the mutant cells (mean ± S.E., $n = 4$ cells; sum of squares *F*-test, $p < 0.05$).

Taken together, our findings show that neither the spatial distribution of munc18 and syntaxin molecules nor that of vesicles is controlled by mode 2/3 interaction. Further work will be required to determine whether munc18 molecules are associated with every membrane-proximal vesicle. These studies will be important to define the molecular machinery required for both vesicle "docking" and for subsequent fusion in intact cells.

Mode 2/3 Interaction Acts on a Specific Pool of Vesicles and Imparts a Greatly Increased Fusion Probability—The change in the membrane distribution of munc18-syntaxin mode 2/3 interactions, but neither the molecular patterning nor vesicle distribution prompted us to analyze in detail the behavior of every vesicle (as opposed to the mean behavior previously analyzed) during maximal stimulation in both wild type- and mutant-rescued cells. This analysis should reveal whether all of the vesicles in a sample behave in an identical manner, or whether there are different types of vesicular dynamics prior to fusion. The majority of single vesicles in munc18-rescued cells (Fig. 4*D*; 64%, $n = 545$ vesicles from seven cells) had a limited displacement distance. The behavior of these vesicles was identical to that observed in the absence of munc18 (*i.e.* in unrescued munc18-silenced cells), suggesting that this pool had no, or few, proximal munc18 molecules. A smaller, more mobile pool of vesicles, comprised 37% of the total vesicle complement and had a greatly increased likelihood of proceeding to membrane fusion (Fig. 4*D*). In total, 75 ± 3% of all single vesicle fusion events (at least 60 fusion events from 6 cells) arose from vesicles contained within this minority pool (*i.e.* a fusion probability enhancement of ~5 times). To further identify any role that mode 2/3 interaction may have in delineating this vesicle behavior (20) and fusion likelihood, we compared these data with those acquired from munc18[I127A]-rescued cells. There was a significant decrease (sum of squares special *F*-test, $p < 0.001$, $n = 8$) in the magnitude of this higher fusion probability pool of vesicles when mode 2/3 interaction was ablated, from 37% to 4% of the total vesicle complement (Fig. 4*D*). These findings correlate with the decrease in exocytosis in I127A-rescued cells. It is noteworthy that the complete removal of this more mobile pool of vesicles was seen upon phosphomimetic mutation of syntaxin serine 14, when these data were analyzed in this manner. This mutation (21) was shown previously to disrupt mode 2/3 interaction and inhibit exocytosis in cells (supplemental Fig. 4). We conclude that the presence of munc18 molecules, engaged in regulated mode 2/3 interaction with syntaxin, exerts a strong positive effect on a specific postdocking pool of vesicles, increasing the probability of fusion by a factor of 5.

DISCUSSION

Despite intensive research the molecular mechanisms behind the docking and priming of secretory vesicles remains poorly defined. It is thought that munc18 acts to promote docking, as in its absence there is a large reduction in the number of

vesicles found immediately adjacent to the plasma membrane of neuroendocrine cells (12, 39, 40), but not in synapses (20). More recently, it was suggested that syntaxin is involved in docking (20) and that t-SNARE heterodimer intermediates act as an acceptor for synaptotagmin (41, 42), forming a docking assembly. In this situation, munc18 has been suggested to act as an ancillary t-SNARE heterodimer-stabilizing factor (13). It is now clear that munc18 is an important factor in the process of both vesicle docking and membrane fusion (*i.e.* postdocking), but the molecular mechanism of its action at the membrane remains undefined. This has been hampered by the lack of available techniques to study this at the molecular and single vesicle level in living samples.

We show that ablating mode 2/3 interaction between munc18 and syntaxin does not reorganize the spatial distribution *per se* of munc18 molecules, or vesicles. We show here that mutating the hydrophobic pocket of munc18 to quantifiably disrupt mode 2/3 interaction with syntaxin results in significant changes in vesicle dynamics and fusion efficiency. Recently, studies have mutated amino acids in or around this region of munc18 and concluded that mode 2/3 interaction has little influence on neuroendocrine exocytosis (10, 43, 44). One of the munc18 amino acid residues targeted in these studies (Glu^{132}, also analyzed here; supplemental figures) (44) was observed to have only modest effects on co-localization with syntaxin compared with Ile^{127}. An additional mutation used in this study (Phe^{115}) (44) was observed to have a low degree of evolutionary conservation (Fig. 1*A*), and we felt it was a poor candidate for subsequent study. From our study, two distinct pools of vesicles can be identified, based on their relative mobility; the majority of fusion events arise from a minority pool of relatively mobile membrane proximal vesicles, which in turn relies on mode 2/3 interactions. Disrupting this interaction reduces the magnitude of this pool and thus immobilizes almost all vesicles at the membrane. How does mode 2/3 interaction between a t-SNARE and an SM protein affect prefusion vesicle dynamics? It is currently thought that munc18 may be part of a larger "docking complex," acting somehow to stabilize the t-SNARE heterodimer (13), which in turn serves as an acceptor for the vesicular synaptotagmin (42). Based on current understanding, this interaction with the assembled SNARE complex would require munc18 to associate with syntaxin in a mode 2/3 interaction. Furthermore, our findings support those in a recent paper (45), which reported that the 4-helical SNARE bundle, containing the syntaxin N-peptide region, is the minimal complement required for munc18-mediated stimulation of membrane fusion *in vitro*. This being the case, it is of interest that different t-SNARE heterodimer conformations are now known to exist (46, 47), with one form stabilized by munc18 association *in vitro* (47). This mechanism would require mode 2/3 interaction. Finally, it was recently reported that munc18 interacts with the v-SNARE synaptobrevin *in vitro* (28), perhaps providing a more direct molecular mechanism for the regulation of vesicle behavior by munc18.

Disruption of mode 2/3 interaction, as well as having an effect on vesicle pool mobility, also interferes with exocytosis from this pool. Again, this is in agreement with findings using phosphomimetic mutation of the N-terminal peptide of syntaxin, which destabilizes mode 2/3 interaction at the plasma membrane. The simplest explanation for these observations is that N-terminal interaction is required for events immediately postdocking and preceding exocytosis. The presence of a munc18 molecule, or molecules, associated with syntaxin (and probably the other SNAREs) is an essential event for exocytosis to proceed. It will now be important to determine whether munc18 molecules are associated with syntaxin underneath every vesicle and how many molecules are there.

Acknowledgments—We thank Shuzo Sugita for providing the munc18-silenced PC12 cells (KD43) and the IMPACT imaging facility, University of Edinburgh, for access to its equipment and software.

REFERENCES

1. Söllner, T., Bennett, M. K., Whiteheart, S. W., Scheller, R. H., and Rothman, J. E. (1993) *Cell* **75,** 409–418
2. Söllner, T., Whiteheart, S. W., Brunner, M., Erdjument-Bromage, H., Geromanos, S., Tempst, P., and Rothman, J. E. (1993) *Nature* **362,** 318–324
3. Sutton, R. B., Fasshauer, D., Jahn, R., and Brunger, A. T. (1998) *Nature* **395,** 347–353
4. Yang, B., Steegmaier, M., Gonzalez, L. C., Jr., and Scheller, R. H. (2000) *J. Cell Biol.* **148,** 247–252
5. Brose, N., Hofmann, K., Hata, Y., and Sudhof, T. C. (1995) *J. Biol. Chem.* **270,** 25273–25280
6. McMahon, H. T., Missler, M., Li, C., and Südhof, T. C. (1995) *Cell* **83,** 111–119
7. Garcia, E. P., Gatti, E., Butler, M., Burton, J., and De Camilli, P. (1994) *Proc. Natl. Acad. Sci. U.S.A.* **91,** 2003–2007
8. Rowe, J., Calegari, F., Taverna, E., Longhi, R., and Rosa, P. (2001) *J. Cell Sci.* **114,** 3323–3332
9. Medine, C. N., Rickman, C., Chamberlain, L. H., and Duncan, R. R. (2007) *J. Cell Sci.* **120,** 4407–4415
10. Arunachalam, L., Han, L., Tassew, N. G., He, Y., Wang, L., Xie, L., Fujita, Y., Kwan, E., Davletov, B., Monnier, P. P., Gaisano, H. Y., and Sugita, S. (2008) *Mol. Biol. Cell* **19,** 722–734
11. Bryant, N. J., and James, D. E. (2001) *EMBO J.* **20,** 3380–3388
12. Voets, T., Toonen, R. F., Brian, E. C., de Wit, H., Moser, T., Rettig, J., Südhof, T. C., Neher, E., and Verhage, M. (2001) *Neuron* **31,** 581–591
13. de Wit, H., Walter, A. M., Milosevic, I., Gulyás-Kovács, A., Riedel, D., Sørensen, J. B., and Verhage, M. (2009) *Cell* **138,** 935–946
14. Gulyás-Kovács, A., de Wit, H., Milosevic, I., Kochubey, O., Toonen, R., Klingauf, J., Verhage, M., and Sørensen, J. B. (2007) *J. Neurosci.* **27,** 8676–8686
15. Fisher, R. J., Pevsner, J., and Burgoyne, R. D. (2001) *Science* **291,** 875–878
16. Dulubova, I., Sugita, S., Hill, S., Hosaka, M., Fernandez, I., Südhof, T. C., and Rizo, J. (1999) *EMBO J.* **18,** 4372–4382
17. Pevsner, J., Hsu, S. C., and Scheller, R. H. (1994) *Proc. Natl. Acad. Sci. U.S.A.* **91,** 1445–1449
18. Toonen, R. F., and Verhage, M. (2003) *Trends Cell Biol.* **13,** 177–186
19. Verhage, M., Maia, A. S., Plomp, J. J., Brussaard, A. B., Heeroma, J. H., Vermeer, H., Toonen, R. F., Hammer, R. E., van den Berg, T. K., Missler, M., Geuze, H. J., and Südhof, T. C. (2000) *Science* **287,** 864–869
20. de Wit, H., Cornelisse, L. N., Toonen, R. F., and Verhage, M. (2006) *PLoS ONE* **1,** e126
21. Rickman, C., and Duncan, R. R. (2010) *J. Biol. Chem.* **285,** 3965–3972
22. Misura, K. M., Scheller, R. H., and Weis, W. I. (2000) *Nature* **404,** 355–362
23. Pevsner, J., Hsu, S. C., Braun, J. E., Calakos, N., Ting, A. E., Bennett, M. K., and Scheller, R. H. (1994) *Neuron* **13,** 353–361
24. Dulubova, I., Khvotchev, M., Liu, S., Huryeva, I., Südhof, T. C., and Rizo, J. (2007) *Proc. Natl. Acad. Sci. U.S.A.* **104,** 2697–2702
25. Shen, J., Tareste, D. C., Paumet, F., Rothman, J. E., and Melia, T. J. (2007) *Cell* **128,** 183–195

26. Rickman, C., Medine, C. N., Bergmann, A., and Duncan, R. R. (2007) *J. Biol. Chem.* **282,** 12097–12103
27. Burkhardt, P., Hattendorf, D. A., Weis, W. I., and Fasshauer, D. (2008) *EMBO J.* **27,** 923–933
28. Xu, Y., Su, L., and Rizo, J. (2010) *Biochemistry* **49,** 1568–1576
29. Deák, F., Xu, Y., Chang, W. P., Dulubova, I., Khvotchev, M., Liu, X., Südhof, T. C., and Rizo, J. (2009) *J. Cell Biol.* **184,** 751–764
30. Graham, M. E., Sudlow, A. W., and Burgoyne, R. D. (1997) *J. Neurochem.* **69,** 2369–2377
31. Rickman, C., and Davletov, B. (2005) *Chem. Biol.* **12,** 545–553
32. Landau, M., Mayrose, I., Rosenberg, Y., Glaser, F., Martz, E., Pupko, T., and Ben-Tal, N. (2005) *Nucleic Acids Res.* **33,** W299–302
33. DeLano, W. L. (2002) *The PyMOL Molecular Graphics System*, DeLano Scientific LLC, Palo Alto, CA
34. Madabushi, S., Yao, H., Marsh, M., Kristensen, D. M., Philippi, A., Sowa, M. E., and Lichtarge, O. (2002) *J. Mol. Biol.* **316,** 139–154
35. Medine, C. N., McDonald, A., Bergmann, A., and Duncan, R. R. (2007) *Microsc. Res. Tech.* **70,** 420–425
36. Zilly, F. E., Sørensen, J. B., Jahn, R., and Lang, T. (2006) *PLoS Biol.* **4,** e330
37. Degtyar, V. E., Allersma, M. W., Axelrod, D., and Holz, R. W. (2007) *Proc. Natl. Acad. Sci. U.S.A.* **104,** 15929–15934
38. Axelrod, D. (2001) *Traffic* **2,** 764–774
39. Toonen, R. F., Kochubey, O., de Wit, H., Gulyas-Kovacs, A., Konijnenburg, B., Sørensen, J. B., Klingauf, J., and Verhage, M. (2006) *EMBO J.* **25,** 3725–3737
40. Verhage, M., and Sørensen, J. B. (2008) *Traffic* **9,** 1414–1424
41. Rickman, C., and Davletov, B. (2003) *J. Biol. Chem.* **278,** 5501–5504
42. Rickman, C., Archer, D. A., Meunier, F. A., Craxton, M., Fukuda, M., Burgoyne, R. D., and Davletov, B. (2004) *J. Biol. Chem.* **279,** 12574–12579
43. Han, L., Jiang, T., Han, G. A., Malintan, N. T., Xie, L., Wang, L., Tse, F. W., Gaisano, H. Y., Collins, B. M., Meunier, F. A., and Sugita, S. (2009) *Mol. Biol. Cell* **20,** 4962–4975
44. Malintan, N. T., Nguyen, T. H., Han, L., Latham, C. F., Osborne, S. L., Wen, P. J., Lim, S. J., Sugita, S., Collins, B. M., and Meunier, F. A. (2009) *J. Biol. Chem.* **284,** 21637–21646
45. Shen, J., Rathore, S. S., Khandan, L., and Rothman, J. E. (2010) *J. Cell Biol.* **190,** 55–63
46. Rickman, C., Medine, C. N., Dun, A. R., Moulton, D. J., Mandula, O., Halemani, N. D., Rizzoli, S. O., Chamberlain, L. H., and Duncan, R. R. (2010) *J. Biol. Chem.* **285,** 13535–13541
47. Weninger, K., Bowen, M. E., Choi, U. B., Chu, S., and Brunger, A. T. (2008) *Structure* **16,** 308–320